IAC-11.A2.2.5

BUBBLE DYNAMICS, OSCILLATION, AND BREAKUP UNDER FORCED VIBRATION IN MICROGRAVITY

Mohammad Movassat

Mechanical Engineering Department, University of Toronto,

5 King's College Road, Toronto, ON, M5S 3G8

movassat@mie.utoronto.ca

Nasser Ashgriz[1], Markus Bussmann[2]

Abstract

Shape oscillation and the translational motion of a single incompressible air bubble under forced vibration in a water container were studied. A 3D level set based flow solver was employed to solve the governing equations for the bubble motion and capture the interface between two fluids. Bubble shapes are characterized by decomposing it to Legendre harmonics. The bubble response is categorized as small amplitude regular oscillations, large amplitude chaotic oscillations, and chaotic oscillations resulting in bubble piercing. In the latter category, a liquid jet forms that penetrates into the bubble core, resulting in a pierced and toroidal shaped bubble.

I. INTRODUCTION

Thermal management and life support systems in microgravity may require phase separation and degasification of fluid mixtures. The separation of a dispersed gas phase within a liquid is a challenging task in the absence of the gravitational field. Vibration of a liquid container with dispersed bubbles induces an external acceleration which can be used to move the bubbles within the liquid [1, 2]. Depending on the level of the induced acceleration, the bubble dynamics will vary from a linear and regular response, to nonlinear and chaotic causing the bubble to breakup.

Forced vibration induces an oscillatory acceleration of the gas bubbles, which results in an oscillatory buoyancy force acting on the bubbles. Such a force causes a bubble to undergo an oscillatory translational motion. In addition, due to a non-uniform pressure distribution, the bubble goes through shape deformation. The pressure variation due to the vibration has a linear profile at any instant in time and as a result, the bubble experiences an oscillatory pressure variation. The translational motion and shape deformation of the bubble are coupled as the two motions affect the velocity field and pressure distribution. In the context of acoustically forced vibration of a spherical bubble, it has been shown that the coupling between the volume oscillations and the translational motion can result in a chaotic bubble behavior provided that the amplitude of the oscillation is large enough [3, 4].

The applied frequency in this work is an order of magnitude smaller than the acoustic resonance frequency (also called the Minnaert frequency). The Minnaert frequency is about 1.6 kHz for the 4 mm diameter air bubble in water that we consider, yet the applied forcing frequency does not exceed 200 Hz. Also, the order of magnitude of the induced velocities is smaller than the speed of sound and so an adiabatic condition will be assumed. As a result, the bubble is assumed to be incompressible and only shape oscillations of the bubble are considered; both regular and chaotic shape oscillations and translational motion are studied.

Since most previous work on bubble oscillation has used an acoustic force rather than vibration to levitate and modulate the volume and shape of the bubble,

1. Mechanical Engineering Department, University of Toronto, ashgriz@mie.utoronto.ca
2. Mechanical Engineering Department, University of Toronto, bussmann@mie.utoronto.ca

any literature review of bubble oscillation phenomena is incomplete without citing such studies. As well, some liquid droplet oscillation studies are cited here because of the similar physics governing bubble and drop shape oscillations. Free shape oscillations of bubbles and drops within another fluid were first studied by Rayleigh [5] and Lamb [6] for small amplitude oscillations of inviscid fluids. Since then, expressions for oscillation frequency have been expanded to account for fluid viscosities [7] and moderate and large oscillations [8, 9]. Effect of amplitude of oscillations on the oscillation frequency and the decay factor of oscillations was investigated by Mashayek and Ashgriz [10] in a study considering small to large amplitude oscillations for fluids with various viscosities. Internal flow within the drop was also studied in their work to describe the mechanism of drop shape oscillations. An important feature of large amplitude oscillations ($\Delta D/D>0.1$), where D is the bubble/droplet diameter and ΔD is the variation in diameter, is the appearance of nonlinear oscillations that cause different modes of oscillations to interact [11-13]. Energy transfer between different modes of oscillations (modes 2, 3, 4, 6) have been reported in studies considering the shape oscillation of a liquid droplet under acoustic forcing, while neglecting translational motion [14, 15].

When translational motion is considered for a liquid droplet, the coupling of this motion and the shape variation of the droplet makes the motion highly nonlinear and possibly chaotic [16], which means that small changes in initial shape and/or location of a droplet affect its response. A chaotic response exhibits non-repeating and aperiodic shapes and motion, instead of regular oscillations.

As the amplitude of the oscillations of a bubble increases, surface tension cannot maintain the equilibrium spherical shape and at the same time, chaotic translational motion appears. This was first referred to as the "erratic dancing of bubbles" [17]. In addition to the pressure variation due to external forcing, the shape oscillation itself propels the bubble due to asymmetries associated with odd harmonics which couple two nonlinear motions [18]. Doinikov [19] studied all three possible motions for a bubble: volume oscillations, shape oscillations, and translational motion, for a bubble levitated in an acoustic field, and concluded that any initial disturbance of any of the three components of the motion causes excitation and dynamic response of the other two. This coupling among nonlinear motions yielded a chaotic bubble response. In the case of large amplitude asymmetric shape oscillations, the inertia force on the bubble from the surrounding liquid can form a liquid jet within the bubble core. When the density ratio between two fluids is large (e.g. 1000/1), the liquid jet can penetrate into the bubble, resulting in a pierced toroidal-shape bubble with a liquid jet within its core [20]. Bubble piercing makes the dynamics of a chaotic response even more complex.

Studies of single bubble response under forced vibration are usually limited to the translational response of the bubble, neglecting shape deformation. Translational motion has been shown to have the same frequency as the forcing vibration, and the amplitude of translational motion varies linearly with the forcing amplitude [21-23]. An experimental study considering both shape variation and translational motion showed that bubble response is nonlinear for large amplitude oscillations, and that a bubble will breakup if the forcing is large enough [24]. Details of the bubble dynamics, motion, and breakup mechanism were not provided.

The present work focuses on an understanding of the bubble dynamics, shape oscillations and translational motion of a bubble under forced vibration. A 3D numerical model was used to model the bubble behavior in response to the forcing. Regular and chaotic responses are characterized and the mechanism of bubble piercing in the case of large amplitude oscillations is described.

II. NUMERICAL METHODOLOGY

The equations governing the motion of incompressible bubbles in a liquid domain are the mass and momentum conservation equations (the energy equation is not needed since adiabatic and isothermal conditions are assumed),

$$\nabla \cdot \vec{V} = 0 \qquad [1]$$

$$\rho\left(\frac{\partial \vec{V}}{\partial t} + \vec{V} \cdot \nabla \vec{V}\right) = -\nabla p + 2\mu\nabla^2\vec{\mathrm{V}} + \rho\vec{\mathrm{g}} + \sigma\kappa\delta\vec{n} \qquad [2]$$

where $\vec{V}$ is the velocity, p is the pressure, ρ is the density and μ is the viscosity of the fluids. $\vec{g}$ is the gravitational acceleration. The forced vibration is imposed by setting $\vec{g} = g_0 cos(2\pi f t)$ with $g_0 = A(2\pi f)^2$ where g_0 is the acceleration amplitude, A is the vibration displacement amplitude and f is the vibration frequency. One-directional vibration is assumed. The last term in the momentum conservation equation corresponds to the surface tension force. σ is surface tension coefficient and κ is the interface curvature. δ is the Dirac delta function which is zero in cells away from the liquid-gas

interface. $\vec{n}$ corresponds to the unit vector normal to the interface. The interface between the liquid and the gas is captured using a level set algorithm, in which a function, φ, is defined such that it has a zero value at the interface. We assume $\varphi < 0$ in the gas region and $\varphi > 0$ in the liquid region. Therefore we have,

The unit normal on the interface, pointing into the liquid, and the curvature of the interface, are:

$$\vec{n} = \frac{\nabla\varphi}{|\nabla\varphi|}\Big|_{\varphi=0} \quad [3]$$

$$\kappa = \nabla \cdot \left(\frac{\nabla\varphi}{|\nabla\varphi|}\right)_{\varphi=0} \quad [4]$$

Since the interface moves with the fluids, the evolution of φ is given by,

$$\frac{\partial\varphi}{\partial t} + \vec{V} \cdot \nabla\varphi = 0 \quad [5]$$

Details of the numerical method and calculation of properties within the cells containing an interface between the liquid and gas can be found in [25]. Equations 1,2, and 5 are discretized on collocated mesh of uniform square cells. A resolution of 64 cells per bubble diameter was used for all results presented in this work, which is $\Delta x=\Delta y=\Delta z=0.0625$ mm for a bubble diameter of $D=4$ mm. To make the solution stable, time steps were limited to $\Delta t<2\times10^{-5}$ sec.

The conservation of momentum equation can be non-dimensionalized by defining the following non-dimensional variables: $t^* \equiv tf$, $\vec{V}^* \equiv \vec{V}/Df$, $p^* \equiv Dp/\sigma$, and $\vec{g}_0^* \equiv \vec{g}_0/Df^2$, and by introducing a characteristic velocity $U \equiv Af$ and a characteristic acceleration $a \equiv Af^2$. Equation (2) then becomes,

$$\frac{\partial\vec{V}^*}{\partial t^*} + \vec{V}^* \cdot \nabla\vec{V}^* = -\frac{A}{D}\frac{1}{Bo}\nabla p^* + \frac{A}{D}\frac{2}{Re}\nabla^2\vec{V}^* + 4\pi^2\frac{A}{D}cos(2\pi t^*) + \frac{A}{D}\frac{\kappa^*\delta\vec{n}^*}{Bo} \quad [6]$$

where A/D is the ratio of the vibration amplitude to the bubble diameter, $Re = \rho UD/\mu$ is the Reynolds number (ratio of the inertia force to the viscous force), and $Bo = \rho aD^2/\sigma$ is the Bond number (the ratio of the applied body force to the surface tension force). A small value of Bo implies that the surface tension will maintain a spherical bubble shape; as Bo increases, the bubble will begin to deform.

In this work we consider the effect of Bo and A/D on the bubble dynamics. Viscous effects are not significant to this problem, and as a result, there is no discussion of the Reynolds number effect.

III. RESULTS AND DISCUSION

A bubble with a diameter $D=4$ mm is centered in a container of size $10\times20\times10$ mm (respectively in the x, y, and z-directions). Water and air are assumed as the two fluids, with properties of $\rho_l=1000$ kg/m^3, $\rho_g=1$ kg/m^3, $\mu_l=10^{-3}$ Pa.s, $\mu_g=10^{-5}$ Pa.s, and $\sigma=0.073$ N/m. Subscripts "l" and "g" correspond to liquid and gas, respectively. The container is vibrated in the y-direction. All boundary conditions are assumed to be no-slip walls. Depending on the amplitude and frequency of the oscillations, A/D and Bo, the bubble response ranges from a linear regular behavior to nonlinear large amplitude oscillations leading to bubble piercing.

Assuming a cosine vibration beginning with an upward acceleration, the induced buoyancy force will be initially downward. As a result the bubble moves downward and due to the incompressibility, pushes the surrounding liquid upward. Since the geometry and the applied force are the same in the x- and z-directions, the flow field will be identical in these directions. During the second quarter period, the induced acceleration is downward, resulting in an upward buoyancy force which decelerates the downward motion of the bubble. At $t=T/2$, the bubble centre of mass comes to rest, although the flow field is not zero within and around the bubble. The upward buoyancy force continues during the third quarter period, resulting in an upward acceleration of the bubble. During the last quarter period, the buoyancy force changes to downward and decelerates the upward motion of the bubble, and results in a zero velocity for the centre of mass at $t=T$. Although the bubble starts the next oscillation period from a zero centre of mass velocity and experiences the same forcing, the flow field and shape of the bubble are different at $t=T$ than at $t=0$, when the spherical bubble had zero velocity. Depending on the deviation from the spherical shape at the end of each period, the forcing during the next oscillation period would further deform the bubble shape.

Regular and Chaotic Oscillations

To illustrate the effect of A/D and Bo, two cases are presented: a small amplitude case with $A/D=0.02$, and $Bo=0.2$ and a large amplitude case with $A/D=0.1$ and $Bo=0.5$. The Reynolds numbers for these cases are 34.2 and 120.8 for small and large amplitude cases, respectively. Figures 1 and 2 illustrate the shape of the bubble as well as the velocity vectors and velocity magnitude contours for the small and large amplitude cases, respectively. Bubble shape, velocity vectors, and contours are shown at $t=T/4$,

T/2. *3T/4*, and *T*. For *Bo=0.2* and *A/D=0.02* the bubble shape remains almost spherical during the oscillation, while for *Bo=0.5* and *A/D=0.1* a dimple forms on the top surface of the bubble at *t=T/2*, that results from the inertia force applied by pushing the fluid above it. At *t=3T/4* the bubble is squeezed and largely deformed from its initial shape. During the last quarter period, when the bubble moves upward while decelerating, the liquid pushes the bottom of the bubble, and forms a dimple there. A comparison of the velocity magnitudes at corresponding times between two cases also shows that higher forcing results in higher bubble velocities. During successive oscillations, large amplitude oscillations continue for the *Bo=0.5* and *A/D=0.1* case, and the bubble behavior becomes chaotic, while in the small amplitude case, the surface tension force is strong enough to maintain the spherical shape of the bubble.

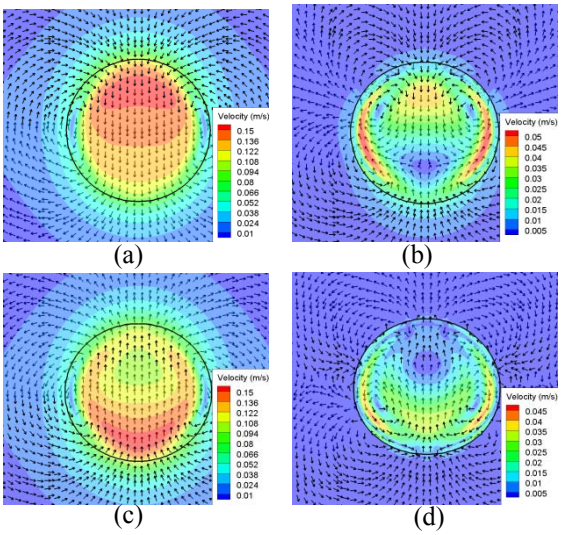

Figure 1: Bubble shape, velocity vectors, and velocity magnitude contours for *Bo=0.2* and *A/D=0.02*, (a) *t=T/4*, (b) *t=T/2*, (c) *t=3T/4*, (d) *t=T*

To characterize the shape oscillation for these two cases, the bubble shapes are decomposed into Legendre polynomials. If the distance from any point on the bubble surface to the centre of mass of the bubble is denoted by *r*

$$r = D/2 + \sum_{n=0}^{\infty} c_n(t) P_n(\cos\theta) \qquad [7]$$

where D is bubble diameter, $P_n(cos\,\theta)$ is the n^{th} mode harmonic, and c_n is the amplitude of the n^{th} harmonic. θ is the polar angle in spherical coordinates. Equations for modes 2 and 3 can be calculated as follows:

$$P_2(cos\theta) = \frac{1}{2}(3cos^2\theta - 1)$$
$$P_3(cos\theta) = \frac{1}{2}(5cos^3\theta - 3cos\theta)$$

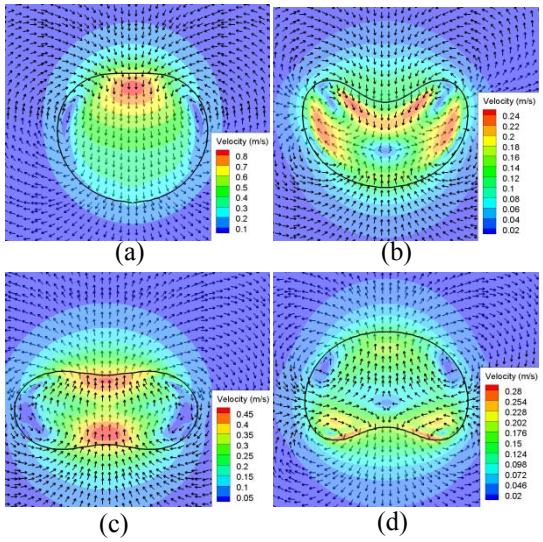

Figure 2: Bubble shape, velocity vectors, and velocity magnitude contours for *Bo=0.5* and *A/D=0.1*, (a) *t=T/4*, (b) *t=T/2*, (c) *t=3T/4*, (d) *t=T*

Even harmonics (*n = 0, 2, ...*) produce shapes which are symmetric with respect to the center of mass; odd harmonics (*n = 1, 3, ...*) are symmetric about the vertical line passing through the center of mass. The time variation of the harmonic amplitudes, c_n, can be used to discern whether the bubble oscillations and deformations are regular or chaotic. If the values of c_n at a certain time in successive oscillations remain constant, the shape will be the same and the oscillations are regular. On the other hand, if the values of c_n do not converge to a constant value but vary at a certain time during consecutive oscillations, the bubble behavior is chaotic and non-repeating. In this section, the first 10 harmonics were calculated. The first two coefficients, c_0 and c_1, were set to zero because c_0 reflects volume oscillation, which was not considered, and c_1 is associated with the bubble center of mass motion. c_2 to c_9 were calculated from the numerical model results using a least squares algorithm [26]. Figures 3 and 4 illustrate the first two coefficients, c_2 and c_3, non-dimensionalized by bubble diameter, for the small and large amplitude cases, respectively. Coefficients are presented at times *t=nT* (*n=1,2,....,50*) which means that the shape of the bubble at the end of each cycle for the first 50 cycles is considered.

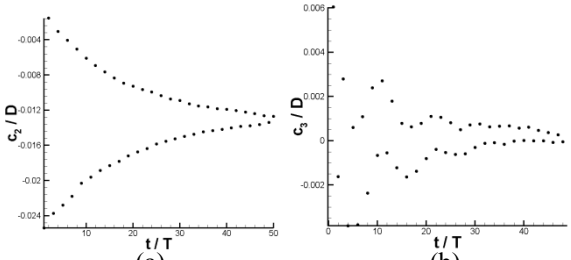

(a) (b)

Figure 3:Time variation of non-dimensional (a) c_2 and (b) c_3 for *Bo=0.2* and *A/D=0.02*, oscillations are regular as the coefficients converge to constant values.

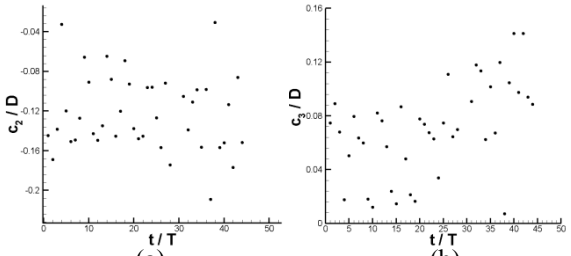

(a) (b)

Figure 4:Time variation of non-dimensional (a) c_2 and (b) c_3 for *Bo=0.5* and *A/D=0.1*, oscillations are chaotic as there is no convergence to a constant value.

For *Bo=0.2* and *A/D=0.02*, the Legendre coefficients converge: c_2/D converges to a value of -0.013 indicating that at the end of each cycle, the bubble shape is slightly oblate, while the convergence of c_3/D to zero indicates that the third mode does not contribute to the bubble shape. For *Bo=0.5* and *A/D=0.1*, c_2 and c_3 are about 10% of the bubble diameter, an order of magnitude higher than the small amplitude coefficients, and there is no convergence after 50 cycles. In this case, the shape variation is nonlinear and non-repeating. Also the excitation of the third mode, which is asymmetric, results in different shape variations on the top and the bottom parts of the bubble; surface tension cannot maintain the symmetric bubble shape, and the bubble behavior becomes chaotic.

Since the shape oscillation and translational motion are coupled, the regular and chaotic responses of a bubble can also be observed by monitoring the location of the bubble centre of mass. This is illustrated in Figure 5 for both cases. The variation of the centre of mass in the y-direction is shown, as the centre of mass location does not change with time in the two other directions. The origin, y=0, is located in the middle of the domain, and the location of the bubble with time is plotted in mm. For the small amplitude oscillations, the bubble drifts about 0.1 mm downward and then the centre of mass locks in place and oscillates about that position. On the other hand, for *Bo=0.5* and *A/D=0.1* bubble drift is large and there is no single position about which the bubble oscillates. The bubble drifts up and down in the first 25 cycles, and then drifts downward dramatically demonstrating a chaotic translational motion.

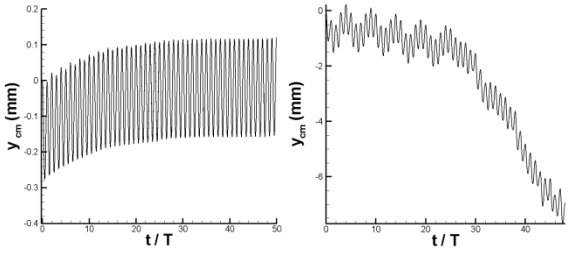

(a) (b)

Figure 5: Bubble centre of mass variation with time in y-direction, (a) *Bo=0.2, A/D=0.02*, (b) *Bo=0.5, A/D=0.1*

Bubble Piercing

The fact that the bubble shape becomes nonlinear, chaotic, and highly deformed provides the opportunity for bubble breakup. It has been observed that due to the inertia of the surrounding liquid for bubbles in acoustic fields undergoing large deformations, a liquid jet can form within the core of the bubble, resulting in a pierced bubble with a toroidal shape [20]. This problem is studied here for a bubble undergoing forced vibration. The forcing is increased to *Bo=0.7* and *A/D=0.125*. Figure 6 illustrates the shape of the bubble as well as velocity vectors at certain times for this case. Vectors are plotted uniformly and velocity magnitude is illustrated by its contour.

During the first quarter period, while the bubble moves downward, the liquid which pushes on the top part of the bubble causes higher bubble velocities close to this region. As well, a very small dimple is formed on the top of the bubble. During the deceleration of the bubble in the second quarter period, the bubble tends to slow down while the denser liquid pushes on the top. The inertia force from the liquid initiates and develops a liquid jet within the core of the bubble. In addition to the liquid inertia force, the Rayleigh-Taylor (R-T) instability condition causes the liquid jet to form rapidly during the second quarter period. The R-T instability occurs when there is an interface between two fluids of different densities located in an accelerating field. If the acceleration and density gradient vectors have the same direction, the interface between two fluids will

be stable. But, if the acceleration and density gradient vectors are in opposite directions, then the interface between the two fluids will be unstable and small disturbances on the interface will grow. During the second quarter period, the acceleration is downward while the density gradient vector is upward on the top surface of the bubble, i.e. the heavier fluid is on top of the lighter fluid. As a result, the top surface of the bubble is unstable based on R-T theory, and any disturbance (which is the dimple formed on the top surface due to the fluid inertia) will grow in time. It can be seen that the liquid jet develops fast during this quarter period. (It should be mentioned that based on R-T theory the bottom surface of the bubble is stable). The unstable condition for the top surface continues during the third quarter period as the direction of acceleration remains downward. At *t=0.66T*, the front of the liquid jet contacts the bottom surface of the bubble, forming a pierced bubble with a toroidal shape.

Viscous Effects

It was mentioned that viscous forces and consequently the Reynolds number are not important in this case and water viscosity is not large enough to affect the bubble behavior. To demonstrate this, in this section the case of *Bo=0.7* and *A/D=0.125* is presented assuming both fluids to be inviscid. This was the case which resulted in bubble piercing. Simulation results show that similar to the viscous case, the liquid jet starts to form on the top surface of the bubble and penetrates the core of the bubble, resulting in a pierced bubble. The bubble shape as well as the flow field and velocity magnitude contours are illustrated in Figure7 for the inviscid case at *t=0.35T* and *t=0.55T,* which can be compared to corresponding results of the viscous case. Although there are small differences in the velocity magnitude contours, the viscous effect is negligible as the shapes of the bubbles are very similar in two cases. To compare the time evolution of the liquid jet penetration in the two cases, Figure8 illustrates the distance from the front of the liquid jet to the bottom of the container. In the inviscid case, the jet front is always further ahead but the difference is very small. The maximum difference between the two cases is about 0.134 mm, which is about two cell widths. Based on this comparison, Bo and A/D are clearly the main non-dimensional numbers governing this bubble oscillation problem.

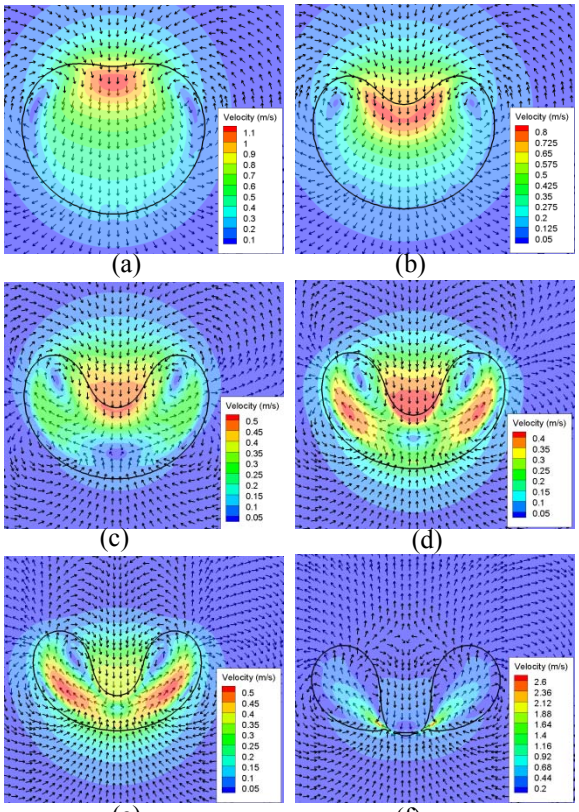

Figure 6: Bubble piercing, bubble shape, velocity vectors, and velocity magnitude contours for *Bo=0.7* and *A/D=0.125* at (a) t=0.25T, (b) t=0.35T, (c) t=0.45T, (d) t=0.5T, (e) t=0.55T, (f) t=0.66T

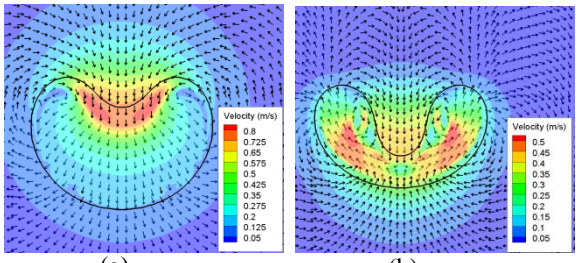

Figure 7: Bubble shape, velocity vectors, and velocity magnitude contours for *Bo=0.7* and *A/D=0.125* at (a) t=0.35T, (b) t=0.55T. Both fluids are assumed to be inviscid. Compared to Figure 6 (b) and (e) viscous forces have negligible effects.

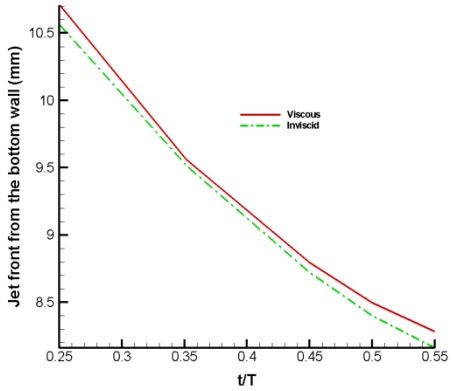

Figure 8: The variation of the distance from the liquid jet front to the container bottom with time, for the viscous and inviscid cases.

Regular oscillation-Chaotic-Piercing map

Since A/D and Bo are the two governing non-dimensional numbers for the bubble oscillation problem, a parametric study was performed to predict the bubble response to forced vibration at various A/D and Bo numbers. Figure 9 illustrates a summary of the results. Three types of responses are characterized: regular oscillations, chaotic oscillations without piercing, and chaotic oscillation with piercing. Piercing cases are chaotic, in which the shape variation and forcing is large enough to pierce the bubble. Three lines are also shown in this Figure. These are constant second, third, and fourth mode resonant frequencies for an air bubble ($D=4$ mm) in water [6]. The corresponding frequencies are 52.6, 96, and 144 Hz, respectively. If the bubble is forced to oscillate at either of the resonance frequencies, the corresponding mode would excite and large amplitude oscillations would occur.

Regular oscillations happen at low amplitudes, $A/D \leq 0.08$, and small buoyancy forces, $Bo \leq 0.4$. In these cases, the shape of the bubble does not undergo large amplitude oscillations, and small amplitude second mode oscillations are observed. The bubble oscillates between small amplitude oblate and prolate shapes, and surface tension force is strong enough to maintain an equilibrium shape of the bubble. Two chaotic-no piercing cases cab be observed within the regular region, $Bo=0.4$, $A/D=0.02$ and $Bo=0.4$, $A/D=0.05$. These two cases coincide with the third and fourth mode resonance frequencies. The forced oscillation excites large amplitude shape oscillations in these cases, while in a larger amplitude case at the same Bond number, the oscillations turn back to regular as the forcing frequency is different from the resonant frequencies. The triangular points correspond to cases in which oscillations are nonlinear with large amplitudes, but there is no piercing of the bubble. Large amplitude shape oscillations make the bubble response chaotic as described for the case with $Bo=0.5$ and $A/D=0.1$. Due to the large shape deformations, the detachment of small bubbles from the main bubble was observed in some of the no-piercing cases. For the no-piercing cases, the oscillations were imposed for 10 cycles without an occurrence of piercing.

As the amplitude of the oscillations and the Bo number increase, the inertia force from the surrounding liquid as well as the R-T instability cause the bubble to be pierced. Simulations were stopped when piercing occurred. Due to the chaotic response of the bubble to large amplitude oscillations, the border between no-piercing and piercing cases is not always predictable. For instance, for $Bo=0.6$, the bubble pierces for $A/D=0.03$, 0.04, and 0.05 while no piercing occurs for larger amplitudes of $A/D=0.06$, 0.07, and 0.08. Analysis of the bubble response showed that the shape of the bubble also has a significant role in the occurrence of piercing. Since the shape variation is chaotic, the case with $Bo=0.6$ and $A/D=0.05$ results in piercing while with the same Bo and $A/D=0.06$ no piercing is observed.

Summarizing our understanding of the occurrence of bubble piercing:

i. Non-symmetric shape oscillations are required for bubble piercing to occur. Non-symmetric shapes are excited when the amplitude of the oscillations is large such that the surface tension cannot maintain the equilibrium shape of the bubble. Large amplitude shape oscillations which are excited due to large amplitude vibrations, large Bo, or the coincidence of the forcing frequency with one of the resonance frequencies, are necessary conditions for the occurrence of bubble piercing.

ii. Due to the large density ratio between water and air, the inertia force from the liquid can highly deform the bubble interface, especially during the deceleration phases of the motion. The parts of the interface where the liquid pushes the gas are more susceptible to the force. The initiation of the formation of the piercing liquid jet is due to the inertia force of the liquid.

iii. The R-T instability enhances the penetration of the liquid jet within the bubble core. Depending on the direction of the acceleration, the top and bottom parts of the bubble are unstable due to the R-T

instability. In the presence of a disturbance, which is usually a dimple formed due to the fluid inertia, the R-T instability can cause the liquid jet to develop rapidly.

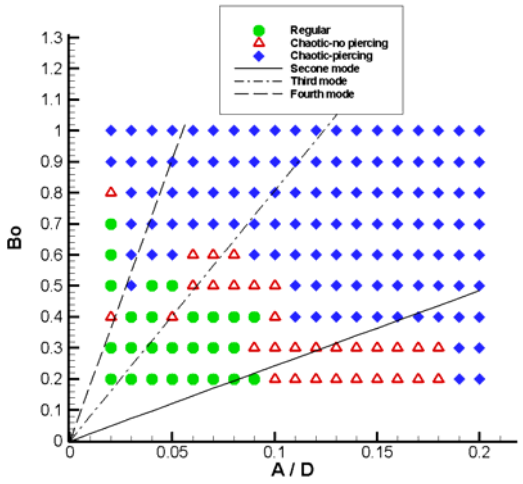

Figure 9: Bubble response to forced vibrations as a function of Bo and A/D. Three types of responses were characterized, regular oscillation, chaotic oscillation without piercing, and chaotic oscillation with piercing. The straight lines are of constant frequency, which correspond to the first three resonant frequencies modes.

IV. CONCLUSION

The response of a single air bubble in a container of water subject to a forced vibration was studied using a numerical 3D model. The coupled shape oscillations of the bubble and its translational motion were considered, but volume oscillations were neglected. The Bond number and the ratio of vibration amplitude to bubble diameter, A/D, were found to be the two governing non-dimensional numbers. Bubble response was characterized in three categories. For small Bo and A/D, the bubble oscillates regularly and the translational motion also shows a regular oscillatory motion. The bubble oscillates between oblate and prolate shapes and there is no appearance of third mode oscillations. As Bo and A/D increase, an asymmetric third mode appears and the bubble shape shows nonlinear, large amplitude, and chaotic oscillations. The amplitude of different mode oscillations can be as large as 10% of the bubble diameter. If the forcing increases, bubble piercing occurs in which a liquid jet is formed and penetrates the bubble core, resulting in a pierced bubble around a liquid core. Chaotic shape oscillation, the inertia of the liquid and the Rayleigh-Taylor instability are responsible for the occurrence of bubble piercing. Finally, a map of bubble behaviour versus Bo and A/D was presented.

REFERENCES

1. Monti, R.: Gravity jitters: effect on typical fluid science experiments, in low gravity fluid dynamics and transport phenomena. AIAA Progress in Astronautics and Aeronautics, 130, 275–307 (1990)

2. Alexander, I.: Impulse, vibrations and random disturbances: consequences for convective diffusive transport and fluid interfaces in low gravity experiments. AIAA 96-2073, presented at 27th Fluid Dynamics Conference, New Orleans, LA, June 17-20 (1996)

3. Akhatov, I. S., Konovalova, S. I.: Regular and chaotic dynamics of a spherical bubble, J. Appl. Math. Mech. 69, 575-584 (2005)

4. Watanabe, T., Kukita, Y.: Translational and radial motions of a bubble in an acoustic standing wave field. Phys. Fluids A 5, 2682-2688 (1993)

5. Rayleigh, L.: On the capillary phenomena of jets. Proc. R. Soc. London 29, 71-97 (1879)

6. Lamb, H.: Hydrodynamics, Cambridge University Press (1930)

7. Miller, C. A., Scriven, L. E., , The oscillations of a fluid droplet immersed in another fluid, J. Fluid Mech. 32, 417-435 (1968)

8. Lundgren, T. S., Mansour, N. N.: Oscillation of drops in zero gravity with weak viscous effects. J. Fluid Mech. 194, 479-510 (1988)

9. Patzek, T. W., Benner, R. E., Bassaran, O. A., Scriven, L. E.: Nonlinear oscillations of inviscid free drops, J. Comput. Phys. 97, 489-515 (1991)

10. Mashayek, F., Ashgriz, N.: Nonlinear oscillations of drops with internal circulations, Phys. Fluids 10 (5), 1071-1082 (1998)

11. Basaran, O. A.: Nonlinear oscillations of viscous liquid drops, J. Fluid Mech. 241, 169-198 (1992)

12. Trinh, E., Wang, T. G.: Large-amplitude free and driven drop-shape oscillations: experimental observations. J. Fluid Mech. 122, 315-338 (1982)

13. Trinh. E. H., Holt, R. G., Thiessen, D. B.: The dynamics of ultrasonically levitated drops in an electric field, Phys. Fluids 8 (1), 43-61 (1996)

14. Trinh, E. H., Thiessen, D. B., Holt, R. G.: Driven and freely decaying nonlinear shape oscillations of drops and bubbles immersed in a liquid: experimental results, J. Fluid Mech. 364, 253-272 (1998)

15. Azuma, H., Yoshihara, S.: Three-dimensional large-amplitude drop oscillations: experiments and theoretical analysis. J. Fluid Mech. 393, 309-332 (1999)

16. Feng, Z. C., Su, Y. H.: Numerical simulations of the translational and shape oscillations of a liquid drop in an acoustic field, Phys. Fluids 9 (3), 519-529 (1997)

17. Eller, A., Crum, L.: Instability of the motion of a pulsating bubble in a sound field, J. Acoust. Soc. Am. 47, 762-767 (1970)

18. Benjamin, T. B., Ellis, A. T.: Self-propulsion of asymmetrically vibrating bubbles. J. Fluid Mech. 212, 65-80 (1990)

19. Doinikov, A. A.: Translational motion of a bubble undergoing shape oscillations. J. Fluid Mech. 501, 1-24 (2004)

20. Blake, J. R., Keen, G. S., Tong, R. P., Wilson, M.: Acoustic cavitation: the fluid dynamics of non-spherical bubbles. Phil. Trans. R. Soc. Lond. A. 357, 251-267 (1999)

21. Ishikawa, M., Nakamura, T., Yoda, S., Samejima, H., Goshozono, T.: Responsive motion of bubbles to periodic g-jitter. Microgravity Sci. Technol. VII/2, 164-168. (1994)

22. Farris, S.C., Bugg, D. J., Gabriel, K. S.: The motion of bubbles in a sinusoidally oscillating liquid in microgravity. Microgravity Sci. Technol. XV/3, 28-35 (2004)

23. Friesen, T. J., Takahira, H., Allegro, L., Yasuda, Y., Kawaji, M.: Numerical simulations of bubble motion in a vibrated cell under microgravity using level set and VOF algorithms. Ann. N.Y. Acad. Sci. 974, 288-305 (2002)

24. Yoshikawa, H. N., Zoueshtiagh, F., Caps, H., Kurowski, P., Petitjeans, P.: Bubble splitting in oscillatory flows on ground and in reduced gravity. Eur. Phys. J. E. 31, 191-199 (2010)

25. Lakehal,D., Meier, M., Fulgosi,M.: Interface tracking toward the direct simulation of heat and mass transfer in multiphase flows, Int. J. Heat and Fluid Flow, 23, 242-257 (2002).

26. Press, W. H., Numerical recipes in FORTRAN : The art of scientific computing, Cambridge University Press (1992)